Chaotic Boundaries of Nematic Polymers in Mixed Shear and Extensional Flows

M. Gregory Forest,[1] Ruhai Zhou,[1] and Qi Wang[2]
[1]Department of Mathematics, University of North Carolina at Chapel Hill, Chapel Hill, North Carolina, 27599, USA
[2]Department of Mathematical Sciences, Florida State University, Tallahassee, Florida, 32306, USA
(Received 6 April 2004; published 17 August 2004)

Chaotic orientational dynamics of sheared nematic polymers is documented in laboratory experiments and predicted by Doi-Hess kinetic theory for infinitely thin rods. We address robustness of rheochaos when simple shear is modified by a planar straining flow, and the macromolecules have finite aspect ratio. We predict persistence of sheared chaotic response up to a threshold straining flow strength and minimum aspect ratio, beyond which chaotic behavior is arrested. More intriguing, a straining component can induce chaos from periodic shear responses.

DOI: 10.1103/PhysRevLett.93.088301 PACS numbers: 83.80.Xz, 05.45.Pq, 83.10.–y, 83.50.Jf

Nematic polymers may exhibit chaotic phenomena in shear-dominated flows in the laboratory (see, e.g., [1–4]) and in both kinetic and mesoscopic models [5–8]. Using the kinetic theory of Doi and Hess, for infinitely thin rods or platelets in pure simple shear, the authors [9] have produced a phase diagram of all stable states and phase transitions in different regions of the dimensionless parameter space (N, Pe). Here N denotes a dimensionless polymer concentration and the Peclet number $\mathrm{Pe} = \dot{\gamma}/Dr$ is the shear rate $(\dot{\gamma})$ normalized by the average molecular rotational relaxation rate (Dr). For the Maier-Saupe potential and a constant rotational diffusion rate, the chaotic region lies within the rectangle $4.7 < N < 5.4,\ 1 < \mathrm{Pe} < 4.5$; orientation-dependent rotational diffusion gives slightly modified bounds [9]. Our goal here is to track the boundaries of the chaotic region of kinetic theory due to two related and unavoidable physical effects: finite molecule aspect ratio and the addition of straining flow in the plane of shear. These boundaries inform the robustness of shear-induced rheochaos of nematic polymers: how anisotropic must the molecules be, and what extensional flow strength is required for the chaotic response to persist or be arrested? Another robustness criterion is the admission of spatial variations; Chakrabarti *et al.* [10] have recently shown persistence of rheochaos for a mesoscopic Landau-de Gennes model with distortional elasticity.

We now briefly review the kinetic theory [11,12]. Let $f(\mathbf{m}, t)$ be the *orientational probability distribution function* (PDF) for rodlike, rigid, extremely high-aspect-ratio spheroidal molecules with axis of symmetry $\mathbf{m}$ on the unit sphere S^2. The Smoluchowski equation with flow field v, nondimensionalized with the rotational diffusivity constant Dr, is

$$\frac{\partial f}{\partial t} = \mathcal{R}\cdot(\mathcal{R}f + \frac{1}{kT} f \mathcal{R}V) - \mathcal{R}\cdot[\mathbf{m}\times\dot{\mathbf{m}} f], \qquad \dot{\mathbf{m}} = \Omega\cdot\mathbf{m} + a[\mathbf{D}\cdot\mathbf{m} - \mathbf{D}{:}\mathbf{mmm}], \nabla \tag{1}$$

where $\mathcal{R} = \mathbf{m}\times\partial/\partial\mathbf{m}$ is the rotational gradient operator; V is the Maier-Saupe potential

$$V = -\frac{3}{2} NkT\,\mathbf{mm}{:}\langle\mathbf{mm}\rangle; \tag{2}$$

the dimensionless flow field for pure simple shear is

$$v = \mathrm{Pe}(y, 0, 0) = (\mathbf{\Omega} + \mathbf{D})\cdot \mathrm{x}; \tag{3}$$

$\mathbf{D}$ and $\mathbf{\Omega}$ are the corresponding rate-of-strain and vorticity tensors; $\mathrm{x} = (x, y, z)$ are Cartesian coordinates with x the flow direction, y the flow-gradient direction, and z the vorticity axis; kT is the Boltzmann factor. The aspect ratio parameter a is defined by

$$a = \frac{r^2 - 1}{r^2 + 1}, \tag{4}$$

where r is the ratio of the rod length or plate thickness to the diameter. Figure 1 shows the relationship between r and a.

In [9,13], the bifurcation diagram is given for $|a| = 1$, i.e., $r = \infty$ or 0. The chaotic parameter region is blown up in Fig. 2. We first characterize the persistence of the chaotic region for physical aspect ratio parameters, $|a| <$

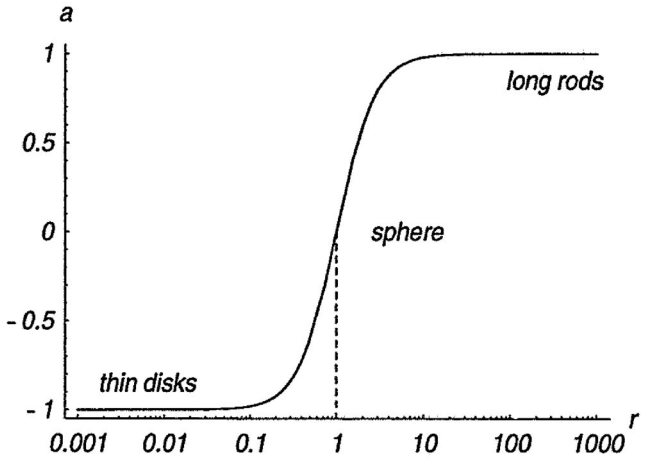

FIG. 1. The shape parameter a versus molecule aspect ratio r.

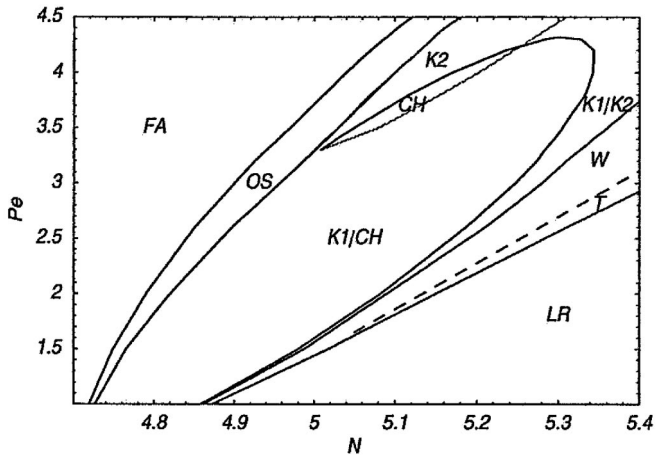

FIG. 2. Bifurcation diagram of all attractors for the parameter domain $4.7 < N < 5.4$, $1 < \mathrm{Pe} < 4.5$ with constant rotational diffusivity and infinite aspect ratio $r = \infty$. Notation: **FA** denotes flow-aligned steady states; **OS** denotes a pair of out-of-plane steady states; $\mathbf{K_1}$ is the kayaking limit cycle in which the peak orientation of the PDF rotates about the vorticity axis; $\mathbf{K_2}$ is a pair of kayaking states in which the peak orientation rotates about a tilted axis; **LR** is the log-rolling steady state; **T** and **W** are the tumbling and wagging states in which the peak orientation rotates or oscillates in the deformation plane; and **CH** denotes a chaotic attractor. Regions with multiple attractors are denoted by $\mathbf{K_1/CH}$ and $\mathbf{K_1/K_2}$.

1. Intuitively, we expect the chaotic region to shrink as the aspect ratio drops. Indeed, lowering $|a|$ is equivalent to adding a straining component to the flow and maintaining the aspect ratio $r = \infty$, a "trade-off" that has been noted by several authors, and precisely formulated in terms of the solution space of kinetic and mesoscopic models in [14,15].

We amplify two vertical slices in Fig. 2 corresponding to fixed nematic concentrations, $N = 5$ and $N = 5.2$, and explore variability with respect to $|a(r)| < 1$. We first write the PDF as a high-order truncated spherical harmonic expansion, and derive a system of ordinary differential equations for each harmonic amplitude [15–17]. Then we employ the continuation software AUTO [18] to identify stable attractors and bifurcation diagrams. Finally we use a 4th order spectral-deferred-correction time-integration method to investigate properties of attracting limit cycles and chaotic orbits. These results determine the attractor taxonomy listed in the caption of Fig. 2; see [8,9,13] for details.

For $N = 5.2$, the bifurcation diagram versus Pe that underlies the phase diagram of Fig. 2 is detailed in Fig. 3(a). From these stable and unstable branches and bifurcations, we employ numerical continuation versus a for fixed $N = 5.2$. The set of all stable states in the parameter rectangle $0.8 < a < 1.13$, $1 < \mathrm{Pe} < 6$ is extracted and compiled in Fig. 3(b). There are nine separate stability regions; in each region all stable state(s) are given. The boundaries of each region are phase transitions of the flowing nematic liquid. The chaotic region is confined within the rectangle $0.98 < a < 1.12$, $1.6 < \mathrm{Pe} < 4.2$.

From Fig. 3(b), for physical aspect ratio parameters $1 < r < \infty (0 < a < 1)$, *the shear rate interval of* Pe *with chaotic attractors contracts as r decreases.* For pure simple shear flow and $N = 5.2$, the critical value at which chaotic response terminates is $|a^*| \approx 0.98$, which corresponds to platelets of aspect ratio $r \approx 10^{-1}$, and rods of aspect ratio $r \approx 10$. For nematic polymers of less extreme aspect ratios, $1/10 < r < 10$, the chaotic range of Pe has vanished at this concentration. The corresponding results of Fig. 3(b) for the $N = 5$ slice of Fig. 2 is given in Fig. 4. Note that we have scaled the axes a and Pe, yet only slightly, and the $N = 5$, 5.2 phase diagrams are remarkably similar.

We emphasize that our methods equally characterize the boundaries in parameter space of other attractors, both steady (**FA**, **OS**) and unsteady (**T**, **W**, $\mathbf{K_1}$, $\mathbf{K_2}$), and also map out regions of unique versus bi- and tri-stability. Note further that we have allowed a to wander outside the apparently physical bounds $|a| < 1$, which now will

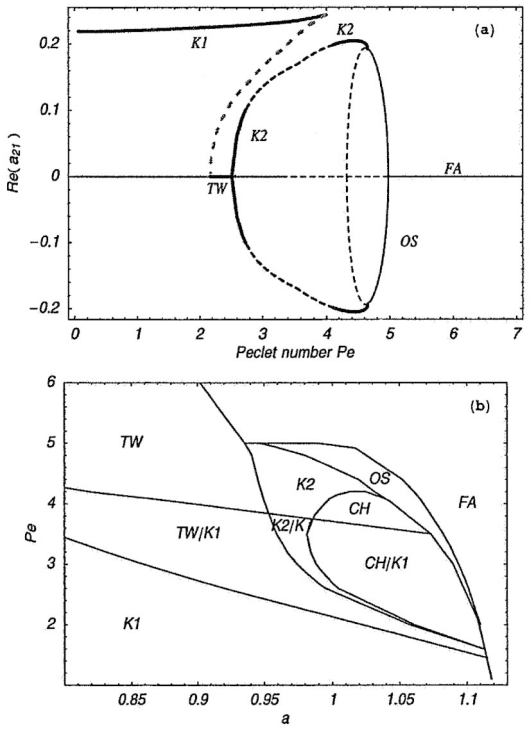

FIG. 3. (a) Bifurcation diagram for the $N = 5.2$ slice of Fig. 2, viewed through the real part of the spherical harmonic amplitude a_{21}, corresponding to aspect ratio parameter $a = 1$, i.e., infinitely thin rods. (b) Phase diagram of all stable states for fixed nematic concentration $N = 5.2$, variable Pe and a. The $a = 1$ slice of the lower figure thus corresponds to the top figure, which establishes parameter contact with Fig. 2 in our numerical continuation framework.

be physically connected in terms of a straining flow perturbation of shear. Consider addition of an arbitrary extensional flow component, for which the dimensionless gradient is

$$\nabla v = \begin{pmatrix} p_1 & \mathrm{Pe} & 0 \\ 0 & -p_1 & 0 \\ 0 & 0 & 0 \end{pmatrix}, \tag{5}$$

where $p_1 = \dot{\varepsilon}/Dr$ is the extensional flow rate ($\dot{\varepsilon}$) normalized by rotational diffusion rate (Dr). The flow parameter ratio p_1/Pe is the ratio of extension rate to shear rate:

$$\chi = \frac{p_1}{\mathrm{Pe}} = \frac{\dot{\varepsilon}}{\dot{\gamma}}. \tag{6}$$

In [14], we formulated a correspondence principle between nematic polymers in general planar linear flow and pure simple shear flow. From that principle, the monodomain response of nematic polymers with aspect ratio parameter a in the flow field (5) is identical to the monodomain response of another nematic polymer liquid with aspect ratio parameter $\bar{a}$ in pure simple shear flow with shear rate Pe, where the molecular aspect ratios are related by

$$\bar{a} = a\sqrt{1 + 4\left(\frac{p_1}{\mathrm{Pe}}\right)^2}. \tag{7}$$

As amplified in [14], $\bar{a}$ need not correspond to a physical molecular aspect ratio; that is, $|\bar{a}| > 1$ is allowable in pure simple shear and simply corresponds to an extensional flow component of a "real liquid" $|a| < 1$ in addition to the shear component Pe .

We now revisit Fig. 3(b) in this light and observe that the phase diagram for $a \geq 1$ is equivalent to fixing $a = 1$, renaming the axis $\bar{a}$ in Fig. 3(b), and admitting a flow field continuation from $p_1 = 0$ to $p_1 = \frac{\mathrm{Pe}}{2}\sqrt{\bar{a}^2 - 1}$ (an equivalent statement of (7) with $a = 1$).

These arguments allow us to transform Fig. 3(b) for $a \geq 1$ into another phase diagram with direct physical relevance. For fixed concentration $N = 5.2$ and extreme aspect ratio ($a = 1$), Fig. 5(a) gives the phase diagram of attractors and phase transitions versus shear rate Pe and the relative strength (χ) of extension rate to shear rate

$$\chi = \frac{p_1}{\mathrm{Pe}} = \frac{1}{2}\sqrt{\left(\frac{\bar{a}}{a}\right) - 1}. \tag{8}$$

(In fact, for any physical aspect ratio, $|a| < 1$, we can give a similar phase diagram using the formula (8).) Note the horizontal axis of Fig. 5(a) coincides with the $a = 1$ vertical slice of Fig. 3(b) and the bifurcation diagram of Fig. 3(a).

Observe from Figs. 2 and 3 and the horizontal axis of Fig. 5(a), for pure simple shear flow $\chi = 0$, the Pe window of chaos is $2.69 < \mathrm{Pe} < 4.1$. As we amplify a small extensional flow component, $\chi > 0$, the chaotic window of Pe grows. The right boundary increases until $\chi \approx 0.1$, then sharply drops as χ approaches 0.25 to hit the left boundary. The left boundary also shows that, when the

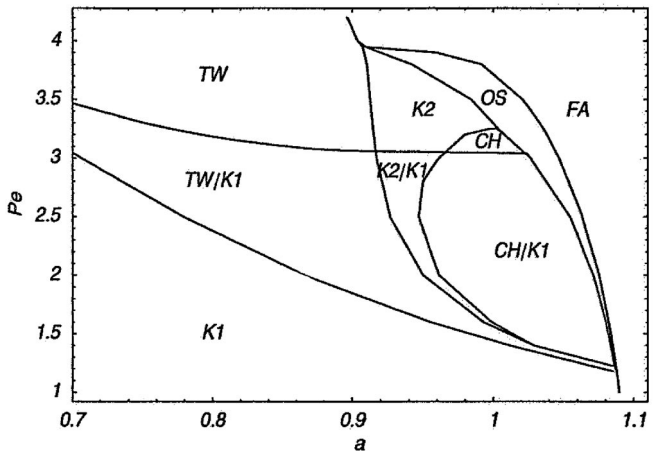

FIG. 4. Phase diagram of all sheared monodomain attractors of the Doi-Hess kinetic theory for fixed nematic concentration $N = 5$. The vertical axis is the normalized shear rate Pe; the horizontal axis is the molecular aspect ratio parameter a.

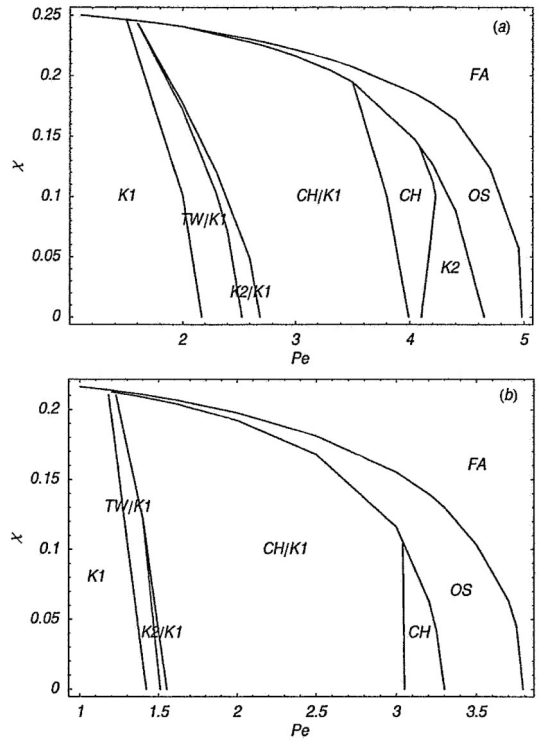

FIG. 5. Phase diagrams for monodomain attractors of Doi-Hess kinetic theory for infinitely thin rods ($a = 1$) at two distinct nematic concentrations, $N = 5.2$ (top) and $N = 5$ (bottom). The horizontal axis is normalized shear rate (Pe), and the vertical axis χ is the ratio of extension rate ($\dot{\varepsilon}$) to shear rate ($\dot{\gamma}$), see Eq. (6).

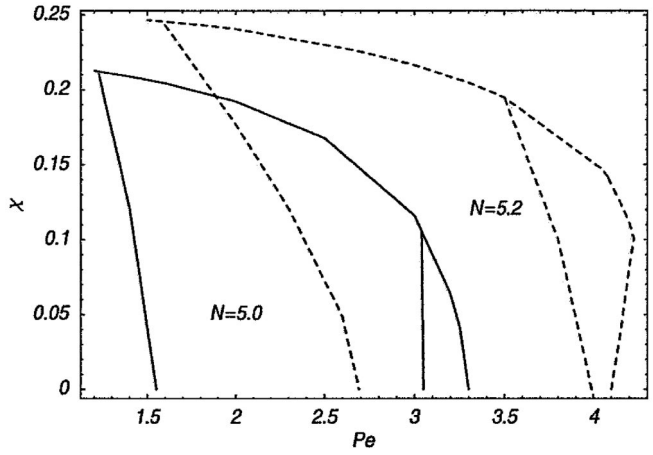

FIG. 6. . Comparison of chaotic regions in the parameter space of normalized shear rate (Pe) and extension rate (χ), for fixed nematic concentrations, $N = 5$ (solid curves) and $N = 5.2$ (dashed curves), and extremely thin rods ($a = 1$).

extension rate ($\dot{\varepsilon}$) approaches a critical value, chaotic dynamics is created from the otherwise periodic monodomain dynamics in pure simple shear. From the phase diagrams of Fig. 5 for either concentration, one can consider a sequence of vertical slices, e.g., Pe = 2.0, 2.4, 2.6 of Fig. 5(a). These slices correspond to the transition sequence of attractors versus $\chi = \dot{\varepsilon}/\dot{\gamma}$, starting from pure simple shear, $\chi = 0$. We find that $\mathbf{T}$, $\mathbf{W}$, $\mathbf{K_1}$, and $\mathbf{K_2}$ attractors all exist for sufficiently weak extension rates, then undergo a transition to chaos as χ increases. Furthermore, the chaotic attractors persist for a finite interval of χ that varies with Pe and N, as detailed in Figs. 5(a) and 5(b). The phase diagram for $N = 5.2$ [Fig. 5(a)] also shows that with $|a| = 1$, for sufficiently strong extension rate, $\chi > 0.25$, chaotic response has been completely arrested, independent of shear rate (Pe).

Finally, we superimpose the chaotic regions for $N = 5$ and $N = 5.2$ on the same (Pe, χ) scales in Fig. 6. This comparison shows how the chaotic flow domain shifts versus concentration, yet remains qualitatively similar. Clearly, one can use these tools to calculate similar phase diagrams for any concentration N and aspect ratio parameter a.

In conclusion, the parameter regime of chaotic orientational dynamics of shear-dominated flowing nematic polymers has been explored with a combination of numerical continuation software and a correspondence principle of the Doi-Hess kinetic theory. The dynamics and phase transitions have been characterized versus molecular composition (concentration and aspect ratio), flow type, and flow rate for a linear combination of planar shear and extension. The chaotic boundaries are mapped out for selected two-dimensional parameter regimes. The chaotic orbits identified previously for infinite aspect ratio rods [5,9] are shown to persist to finite aspect ratios on the order of 10. An intriguing prediction emerges from our numerical phase diagram: the addition of an extensional flow component at subcritical shear rates can resonate chaotic flow response in an otherwise periodic attractor, including tumbling, wagging, and out-of-plane kayaking limit cycles. On the other hand, any given chaotic response for a fixed parameter set can be driven into a regular, flow-aligned orientational distribution by addition of a finite straining component to the flow. Taken together, these results indicate a degree of robustness as well as intrigue in phase flows of nematic polymers.

Effort sponsored by AFOSR Grant No. F49620-02-1-0086; NSF Grants No. DMI-0115445, No. DMS-0204243, No. DMS-0308019; and by NASA University Research, Engineering and Technology Institute on Bio Inspired Materials (BIMat) under Contract No. NC-1-02037.

[1] A. K. Sood, R. Bandyopadhyay, and G. BasappaPramana **53**, 223 (1999).
[2] R. Bandyopadhyay, G. Basappa, and A. K. Sood, Phys. Rev. Lett. **84**, 2022 (2000).
[3] R. Bandyopadhyay and A. K. Sood, Europhys. Lett. **56**, 447 (2001).
[4] Z. Tan, and G. C. Berry, J. Rheol. (N.Y.) **47**, 73 (2003).
[5] M. Grosso, R. Keunings, S. Crescitelli, and P. L. Maffettone, Phys. Rev. Lett. **86**, 3184 (2001).
[6] G. Rienacker, M. Kroger, and S. Hess, Phys. Rev. E **66**, 040702 (2002).
[7] G. Rienacker, M. Kroger, and S. Hess, Physica A (Amsterdam) **315**, 537 (2002).
[8] M. G. Forest and Q. Wang, Rheol. Acta **42**, 20 (2003).
[9] M. G. Forest, Q. Wang, and R. Zhou, Rheol. Acta (to be published).
[10] B. Chakrabarti, M. Das, C. Dasgupta, S. Ramaswamy, and A. K. Sood, Phys. Rev. Lett. **92**, 188301 (2004).
[11] M. Doi, J. Polym. Sci., Polym. Phys. Ed. **19**, 229 (1981).
[12] S. Hess, Z. Naturforsch., A: Phys., Phys. Chem., Kosmophys. **31A**, 1034 (1976).
[13] M. G. Forest, Q. Wang, and R. Zhou, Rheol. Acta **43**, 17 (2004).
[14] M. G. Forest, Q. Wang, R. Zhou, and E. P. Choate, J. Non-Newtonian Fluid Mech. **118**, 17 (2004).
[15] M. G. Forest, R. Zhou, and Q. Wang, Phys. Rev. E **66**, 031712 (2002).
[16] R. G. Larson and H. C. Ottinger, Macromolecules **24**, 6270 (1991).
[17] V. Faraoni, M. Grosso, S. Crescitelli, and P. L. Maffettone, J. Rheol. (N.Y.) **43**, 829 (1999).
[18] E. J. Doedel *et al.*, Continuation and bifurcation software for ordinary differential equations, computer code AUTO97, Concordia University, (1997).